Combustor-Turbine Interactions by Using the Open National Combustion Code (OpenNCC) and the Glenn-HT Code

Kenji Miki[1] *, Ali Ameri[1,2] †, Thomas Wey[1] ‡, Jeffrey Moder[1] §Mark Celestina[1] ¶

[1] *NASA Glenn Research Center,Cleveland, Ohio 44135, USA*

[2] *The Ohio State University,Columbus, Ohio 43210, USA*

We develop the methodology of coupling two different computational fluid dynamic (CFD) codes, OpenNCC and Glenn-HT, in order to investigate the unsteady flow fields inside the combustor and around the first-stage stator of a high-pressure turbine (HPT) from the energy efficient engine (E^3) program. In our coupling strategy, OpenNCC, a time accurate unstructured mesh multi-phase combustion CFD code, is applied to the combustor region and Glenn-HT, a structured mesh CFD code designed for turbine applications, is utilized inside the HPT region. As a proof of concept, we first simulate the three-dimensional airflow over the backward facing step and compared the predicted pressure coefficient against experimental data. We then considered a Jet-A/Air combustor with the NASA single learn direct injector (LDI) as a reacting flow test case. Here, Glenn-HT is used in the downstream of the combustor and assumes that the working fluid is a single gas (i.e., air) where the properties of the gas are taken from time- and area-averaged values at the combustor exit. A fully coupled combustor-turbine simulation using both OpenNCC and Glenn-HT was conducted on the E^3 combustor and a detailed analysis done pertaining to how a realistic combustor outflow affects migration of hot-streaks and its impact on the aerodynamic behavior inside the HPT. It is found that the combustion dynamics (i.e., the switching main and pilot flame strength) significantly alters the aerodynamic behavior inside the HPT including hot-streak migration. Variations of the temperature and the velocity magnitude in the passage could be up to ± 75 and ± 15. These large variations are an important part of the combustor-turbine interactions, which are overlooked by a single component simulation of the HPT while imposing the steady inflow boundary condition at the HPT inlet. Finally, it is observed the strong density gradient associated with the hot-streaks and the pressure gradient at the passage significantly enhances the baroclinic torque, affecting the vorticity field.

I. Introduction

To improve jet engine efficiency, it is desirable to increase temperature and pressure entering the combustor. As a consequence, the inlet temperature in a high pressure turbine (HPT) is getting close to the metal's melting point requiring the careful introduction cooling air to protect the metal surface. Accurate prediction of turbine flow fields is therefore critical for a successful design process of the HPT. Although modern combustor is designed for efficient fuel–air mixing and a relatively uniform exit temperature profile, Radomsky and Thole[1] investigated the characteristics of both temperature and velocity profiles at the turbine inlet on a single nozzle guide vane (NGV) and reported that the turbulence intensity (Tu) at the combustor exit could be up to $sim40\%$. This strong turbulent motion significantly increases the end-wall heat transfer. In addition, it is necessary to take into account the severe temporal non-uniformity of temperature (so-called, "hot-streaks".)

*Aerospace Engineer of Turbomachinery and Turboelectric Systems Branch

†Senior research scientist of Turbomachinery and Turboelectric Systems Branch

‡Aerospace Engineer of Combustion Branch

§Combustion Branch Chief

¶Turbomachinery and Turboelectric Systems Branch Chief

There have been several noticeable experimental and numerical efforts conducted for a better understanding of hot-streaks. In the 1980s, NASA Lewis Research Center built the Combustor Exit Radial Temperature Simulator (CERTS)[2] aiming at the generation of a realistic non-uniform inlet condition for the HPT in order to understand the hot-streaks. Using the profiles from the CERTS, Dorney *et al.* [3,4] experimentally and numerically observed that hot streaks altered an angle of attack and generated the secondary flows, and Stable and Schwab[5] reported that there are larger pressure losses due to the boundary layer growth compared with the case using a uniform inflow. At the United Technology Research Center (UTRC), the Large Scale Rotating

At the United Technology Research Center (UTRC), the Large Scale Rotating Rig (LSRR) was the large scale rotating rig with an inlet temperature distortion while keeping the uniform total temperature at the inlet.[6] The experimental results showed that the rotor flowfield was greatly affected by the rotor flowfield due to the secondary flow. Similarly, experimental results obtained from the Multi-stage Axial Turbine Research Facility (LISA) also showed that hot streaks induced secondary flows and that hot-streak clocking led to a heat load redistribution.[7] A non-reacting combustor simulator for the Oxford Turbine Research Facility (OTRF) [8] was designed to produce a range of engine realistic swirl and temperature distortion profiles in the upstream of the NGV. Qureshi *et al.* [9] and Hall *et al.*[10] compared the predictions using RANS and URANS simulations with the data from OTRF and addressed the importance of a precessing vortex core (PVC) and vortex breakdown, which could be significantly altered by heat release by combustion. Recently, Adams *et al.* [11] reported the data from the OTRF updated by adding a new non-reacting lean-burn combustor simulator and numerically found that the change in the aerodynamics of the HPT vane and rotors were mainly controlled by the inlet swirl profile and the inlet total temperature profile, respectively. Jacobi *et al.*[12] performed LES simulations including the swirl-generators, transition duct and the four NGV (Tu=10-20%). It was shown that the vortex structures from the swirler fluctuated the horse-shoe vortex and altered its convection process at the vane passage. Based on the experimental data acquired at the Turbine Research Facility (TRF) of the Air Force Research Laboratory (AFRL), Barringer *et al.*[13] performed RANS simulations to investigate the migration of hot-streaks. It was observed that the presence of a hot streak could lead to $\sim 25\%$ variation of heat transfer along the 1^{st} stage rotor vane compared with the uniform HPT inlet conditions. Finally, in European Union, the Full Aerothermal Combustor-Turbine interactions Research (FACTOR) project built a full annulus non-reacting combustor rig, aiming at a better understanding of aero-thermal fields, between the combustor and the HPT.[14] This combustor simulator generates up to $25-30\%$ turbulent intensity at the combustor exit (P40),[15] and the data has been used as a challenging CFD validation data (e.g.,[16–19]). These experimental and numerical results suggest that the simulated non-reacting flow could have fundamental structural difference from the reacting case although these works introduced a realistic swirling flow mimicking an actual combustor outflow. To capture unsteadiness and non-uniformity of the reacting flow fields generated by a real combustor, it is necessary to perform fully-coupled combustor and HPT experiments and simulations.

To the best of author's knowledge, there is no fully-coupled combustor and HPT experimental data available in the context of combustor-turbine interactions. There are, however, many good numerical studies performing the coupling combustor/HPT simulations . Schluter *et al.*[20] performed a Large-eddy simulation (LES)-RANS hybrid simulation for modeling the combustor and the HPT. Medic *et al.*[21] also worked on the integrated simulation coupling the multiple in-house solvers for simulating different components (compressor, combustor, and turbine); in their study, the compressor and turbine were simulated with a RANS solver and the combustor with an LES solver (The similar hybrid approach was also adapted by Verma *et al.*[22] using the commercial CFD solver, ANSYS Fluent.) Roux [23] performed LES simulations for the fully-coupled combustor and high-pressure stators (HPS). Compared with the case without the HPS, they observed that the amplitude and frequencies of the most intense modes of the pressure fluctuations in the combustion chamber were significantly different when the HPS was included. Xia *el al.*[24] investigated hot-streaks migrating with different clocking positions with a coupled combustor/HPT simulations using URANS with FLUENT (a commercial CFD code) and Delayed Detached Eddy Simulation (DDES) with the in-house code, UTCFD for the combustor and the HPT, respectively. Grün*dler el al.*[25] investigated the combustor turbine interactions by comparing the flow fields passing NGV using the unsteady boundary condition created by the Proper Orthogonal Decomposition and Fourier Series (PODFS). Although this approach is computationally affordable and creates a more realistic interface, this approach is unable to capture a dynamic behavior (e.g., combustion dynamics by pressure waves reflected at the stators[26]).

At the National Aeronautics and Space Administration (NASA) Glenn Research Center (GRC), we have

been developing fully-coupled unsteady simulations of combustor-turbine interactions for a realistic geometries of combustor and HPT designs from the 1980's E^3 program (using the General Electric combustor from that program).[27–29] In our previous studies,[26,30–32] we investigated the impact of performing fully-coupled combustor/HPT simulations relative to sequential (one-way coupled) combustor and HPT simulations at two operating conditions (i.e., the simulated sea-level take-off (SLTO) condition and a more realistic SLTO condition) using the in-house code, OpenNCC. In ,[26] we observed that the HPT efficiencies can differ significantly between sequential single-component simulations and fully-coupled combustor/2 stage HPT simulations. It was also shown that there are larger oscillations in the time-history of the HPT efficiency for the fully-coupled simulation. This seems to be attributed to the temperature fluctuations in time from the combustor exit flow.

In this work, we combine two in-house codes, OpenNCC and Glenn-HT to investigate the unsteady flow fields inside the E^3 combustor and the HPT (1^{st} stage only) in terms of hot-streak migration around the 1^{st} stage stator. The Glenn-HT code, which is developed in the Turbomachinery branch at NASA-GRC is designed to specifically investigate aerodynamics inside a turbine. The main feature of the Glenn-HT code is a high-order (less dissipative) three-dimensional compressible Navier-Stokes solver with a variety turbulence models such as, (U)RANS and LES with the sub-grid closure, using structured multi-block grids. The code also has the capability of modeling a conjugate heat transfer and cooling air flows including internal flows inside a blade. The proposed work is similar to the recent study done by Zhang and Lei[33] who investigated two coupling approaches using ANSYS Fluent and CFX. The first coupling approach is that two codes exchange the information at interface-only, and the other approach uses the overlap-zone. The validations were done using the steady calculation with RANS for both the combustor and the HPT (the detailed information of the geometry is not available). Although their coupling scheme using the interface only is close to this work, the main difference is that we propose to run both codes in an unsteady manner so that this is a more natural way to capture unsteady phenomena (such as combustion dynamic, hot streaks migration, etc.) while investigating the combustor-turbine interactions. This work is the first step toward ultimate objective of performing a full-engine (compressor, combustor and turbine) simulation by fully coupling different codes.

This paper is organized as follows. In Sec. II, we explain the proposed coupling methodology after brief descriptions of OpenNCC and Glenn-HT. In Sec. III, we first show the numerical results from two test cases (proof of concept): one is the non-reacting three-dimensional backward facing step and the other is a Jet-A/Air combustor with the single learn direct injector (LDI), and then present the results of the combustor turbine interactions using the E^3 combustor and HPT geometries. The test condition is a realistic sea-level takeoff condition ($P_{S,41}$ =27.4 [atm]). Unlike the previous study[32] where the effect of the boundary layer (i.e., viscous effect) were not well-captured using a relatively coarse mesh, the detailed analysis of unsteady aerodynamics around the first stator of the HPT including the boundary layer and the hot streak migration is provided. Conclusions are then summarized in Sec. VI.

II. Coupling Methodology

In this study, we use the OpenNCC code (the releasable version of the National Combustion Code) for the combustor and the Glenn-HT code for the turbine, both of which have been continuously updated for more than two decades at the NASA Glenn Research Center at the Engine Combustion and Turbomachinery branch, respectively.

1. Combustion Modeling with OpenNCC

OpenNCC is used to simulate the flow fields inside the E^3 combustor, which involves multi-physical phenomena, such as liquid fuel atomization and vaporization, turbulence transport processes and combustion. OpenNCC is equipped with turbulence models (e.g., (U)RANS and LES with sub-grid model[34]), a finite rate chemistry model with turbulent combustion models (the PDF transport model,[35] the Eddy-Breakup Model (EBU),[36] the dynamic thicken flame model (DTF)[37,38]), and the Linear-Eddy Model (LEM)[39]). Liquid fuel is injected as parcels representing a number of real droplets through multiple injection points and in a stochastic manner to mimic a hollow cone distribution. The liquid spray solver is based on a Lagrangian scheme and well-established models for droplet drag and vaporization.[40] Many previous papers and presentations have shown that the combustion CFD capabilities of OpenNCC (as well as NCC) have facilitated the development/design of combustion technology at NASA GRC.

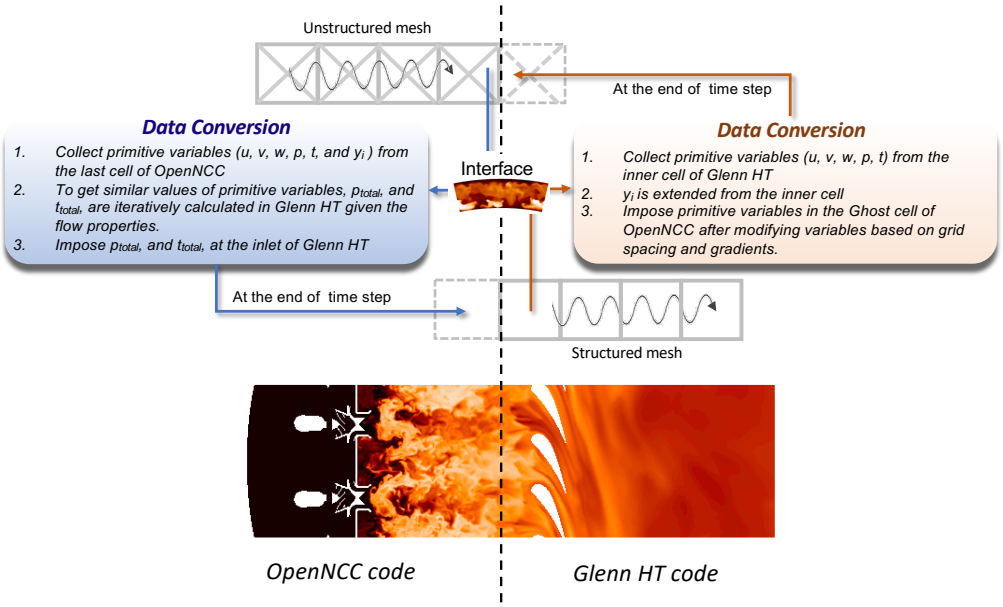

Figure 1. Schematic of the proposed methodology of coupling OpenNCC and Glenn-HT at an interface.

2. High-Pressure Turbine Modeling with Glenn-HT

To investigate the hot-streaks migration around the 1^{st} stage stator of the E^3 HPT, we utilize the Glenn-HT.[41] Glenn-HT solves unsteady non-reacting compressible Navier-Stokes equations using structured multi-block grids under a massively parallel environment. Similar to OpenNCC, it also uses a dual time-stepping procedure, and the explicit four-stage Runge-Kutta scheme is called in pseudo-time is adopted. The transport equations are spatially discretized using a cell-centered finite volume method. The 2^{nd} order AUSM+-up scheme[42] with MUSCL is used to calculate the inviscid flux, thus minimizing the numerical dissipation. A variety of turbulence models are available in Glenn-HT (e.g.,[43–46]) as well as LES with the sub-grid model.[34] Thus, Glenn-HT has been validated against a variety of turbomachinery applications (e.g.,[47–49]) and been proved to accurately predict complex aerodynamic phenomena inside a turbine, such as secondary flows, separation, reattachment and transition. In addition, Glenn-HT is capable of modeling conjugate heat transfer (CHT) problems.[50]

3. Coupling OpenNCC and Glenn-HT

To couple two codes at an interface, it is required to implement "unsteady" boundary conditions in both OpenNCC and Glenn-HT. As an example, when modeling the unsteady flow fields inside the E^3 combustor and the HPT, the unsteady outflow profile at the combustor exit predicted by OpenNCC is collected at each time step, and the exit profile are simultaneously imposed at the HPT inlet while Glenn HT simulates the unsteady flow inside the HPT. One of the main challenges to couple two codes is that OpenNCC and Glenn-HT have different computational domain using different mesh types (i.e., OpenNCC uses the unstructured mesh for the combustor and Glenn-HT uses the structured mesh). In addition, OpenNCC is used to simulate the spray-fuel combustion while Glenn-HT considers only hot air (i.e., the species equation is not solved). Therefore, the gas properties at an interface are not the same. This issue is particularly important since OpenNCC needs the exit boundary condition such as a static pressure, and using a mismatch exit boundary condition from Glenn-HT can results in unphysical pressure waves reflected at the interface. Our previous study[26] using OpenNCC for both the E^3 combustor and the HPT suggests that capturing any dynamics near and within the turbine first-stage stator can be accurately captured only when the combustor and turbine are tightly coupled. Therefore, it is critical not to generate any unphysical dynamics (e.g., pressure waves) at an interface when using two different codes to investigate the combustor-turbine interactions. The coupling

methodology developed in this study is summarized as follows:

1) At each time step, the primitive variables (u, v, w, p_s, T_s, Y_i, and k) from the cell center of the cell including the exit interface (i.e., combustor exit) are collected from OpenNCC.

2) Since Glenn-HT only considers the (hot) air (Y_i is not used) inside the HPT, the gas properties (e.g., Cp, γ, molecular weight, etc.) need to change from the combustor. Given the gas properties of air, it is necessary to iteratively calculate T_{total} and P_{total} to get the same values of primitive variables from OpenNCC. The calculated T_{total} and P_{total} and k are imposed at the ghost cell, which is outside of the interface (i.e., HPT inlet) of Glenn-HT.

3) From the cell center of the cell including the inlet interface, the primitive are collected from Glenn-HT and imposed at the ghost cell, which is outside of the interface (i.e., combustor exit) of OpenNCC.

4) Y_i is extended from the inner cell assuming that the reaction is over at the combustor exit; this assumes the hot gases are at chemical equilibrium

5) 1) – 4) are repeated at the last iteration of each implicit time-stepping.

An obvious drawback of this process is that Glenn-HT assumes the working gas not the combustion products, but hot air. Note that solving Glenn-HT without the species equations, grants enough speed up to allow a detailed analysis of the airflow inside the HPT using a fine mesh. Although the time-history of the area averaged molecular weight and γ are relatively constant at the E^3 combustor exit, these quantities are not constant at a local point. Therefore, the assumption of using the constant molecular weight and γ across the interface needs to be examined carefully. To take into account a difference in grid spacings/types between two meshes used in the combustor and the HPT, the primitive variables are calculated by using a linear interpolation based on the local gradients of valuables. Lastly, in the MPI parallel programming environment, we need to use the following command to submit two different codes at the NASA Advanced Supercomputing (NAS): ***mpiexec -np 12 ./OpenNCC.x : -np 8 ./Glenn-HT.x***, where we use 12 cores for OpenNCC and 8 cores for Glenn-HT. In addition, each code requires to include the following command: call **call *MPI_Comm_split*** when it initiates the MPI environment.

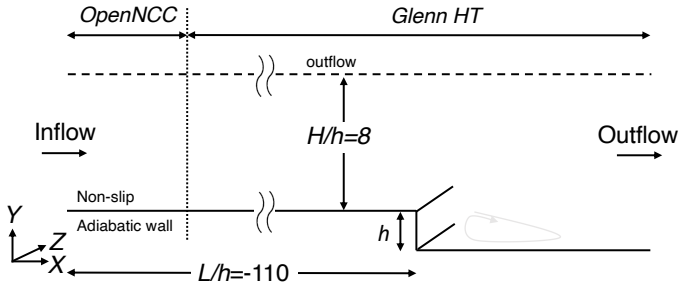

Figure 2. Schematic of the backward facing step with the operating conditions.[51]

III. Proof of Concept

In this section, we perform two test cases for the purpose of the validation and verification of the proposed coupling methodology. The first test case is to simulate the non-reacting flow fields over the three-dimensional

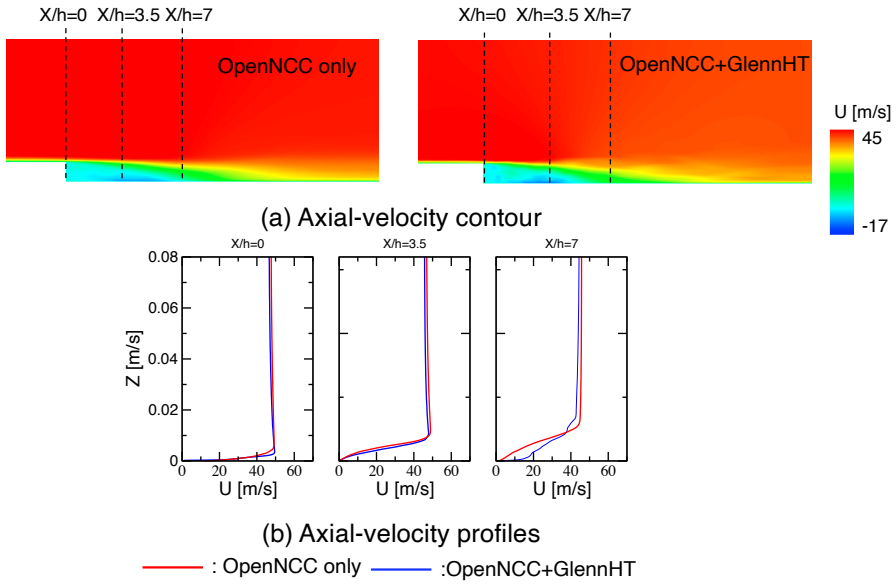

Figure 3. Axial velocity contour (top) and Axial velocity profile at three different axial locations: $X/h = 0$, $X/h = 3.5$, **and** $X/h = 7$.

backward facing step and to compare numerical results (pressure coefficient profile at the bottom wall) predicted by OpenNCC only and both OpenNCC (upstream)/Glenn-HT (downstream) against the experimental data. Structured meshes are used for both domains. The second test case is to model a single-cup lean direct injector (LDI) combustor. This is a relatively complex geometry including an axial air swirler. Gaseous fuel jet ($(C_{11}H_{21})$) is injected from the tip of the swirler, and the reaction takes place at the shear layer where flame is stabilized and hot produced at the recirculation zone. We use an unstructured mesh for the combustor (upstream) modeled by OpenNCC and a structured mesh for the downstream region modeled by Glenn-HT. For both simulations, we use 280 cores (240 cores for OpenNCC and 40 cores for Glenn-HT) (Xeon E5-2680v2) of Pleiades at NASA Advanced Supercomputing facilities. The second-order AUSM+-up scheme[42] with the minmod function as the limiter of the MUSCL is used for calculating the convention term, and the implicit time stepping (with the explicit four-stage Runge-Kutta scheme) is used to advance the solution. For the turbulence model, large eddy simulation (k-equation model) is used. (the authors are aware that the grid resolution used in these studies might be too coarse for adequately resolving small-scale turbulence especially near a wall)

A. Test Case 1: Backward Facing Step

The schematic of the computational domain of the three-dimensional backward facing step is shown in Fig. 2.. In this test case, M=0.128 air flow is introduced from the left boundary, and the turbulent boundary layer is established while flowing in the long channel (L/h=110, where L is the length between the inlet and the backward facing step, and h is the step heigh). The boundary layer experiences the step, forming the flow separation, shear layer and recirculation zone at this step. The reattachment occurs downstream of the step. It is known that the reattachment distance, where the pressure coefficient (Cp) at the bottom wall raises, is sensitive to the numerical setting (e.g., turbulence model, incoming flow at the step, etc.) OpenNCC is used in the upstream region where the boundary layer is developing, and Glenn-HT simulates the flow field around the step. As a quality check, we compare two results from (1) OpenNCC only (i.e., OpenNCC is used for the entire domain) and (2) OpenNCC and Glenn-HT. Figures 3 (a) and (b) show the time-averaged axial velocity contours and the axial velocity profiles at three different axial locations ($X/h = 0$, $X/h = 3.5$,

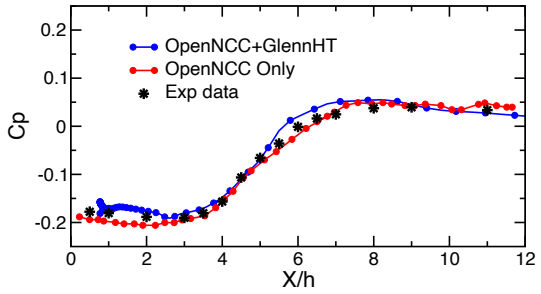

Figure 4. Pressure Coefficient at the wall predicted by (red) OpenNCC only and (blue) OpenNCC and Glenn-HT with the experimental data.[51]

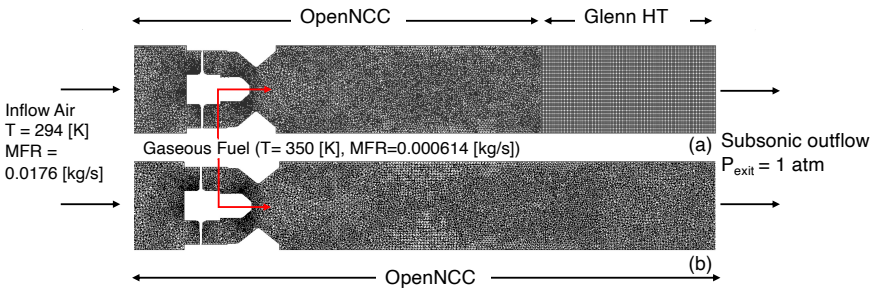

Figure 5. Boundary condition and meshes of a single-cup LDI combustor for (top) OpenNCC and Glenn-HT and (bottom) OpenNCC only.

and $X/h = 7$). Although there are some discrepancies in the reverse flow magnitude inside the recirculation bubble, reasonable agreement between two results is achieved in terms of the boundary layer thickness as well as the shape of the recirculation bubble. More importantly, we observed that the predicted pressure coefficient profiles at the bottom wall agrees well with the experimental data.[51] We also confirmed that the pressure waves smoothly propagated at the interface (not shown here) when coupling OpenNCC and Glenn-HT in an unsteady manner.

B. Test Case 2: LDI Combustor

The second test case is an unsteady chemical reacting case of a single-cup Lean Direct Injector (LDI) combustor. The computational domain/mesh and the boundary conditions are shown in Fig. 5. The constant air flow with a fixed mass flux and temperature (MFR=0.0176 [kg/s], T_{air}=294 [K]) is introduced from the left, goes through the swirler, and mixes with the gaseous fuel ($C_{11}H_{21}$) injected at the tip of the swirler The mass flux and temperature of the fuel are held at 0.000614 [kg/s] and 350 [K], respectively. A subsonic exit boundary condition (P_{exit} = 1 [atm]) is imposed at the left of the Figure. Two simulations were performed at these conditions. The first uses both OpenNCC for the combustor and Glenn-HT for the downstream region.

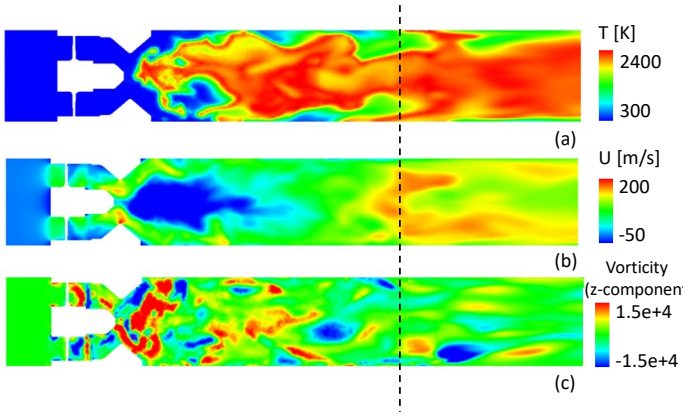

Figure 6. Instantaneous contours of (a) temperature, (b) axial velocity and (c) z-component of vorticity. The dashed line indicates the interface between two domains using OpenNCC and Glenn-HT.

The second uses OpenNCC alone for the entire computational domain. Please note that an unstructured, tetrahedral mesh is used in the combustor region for both cases. Therefore, it is important to ensure that the flow properties smoothly propagate through the interface where structured and unstructured meshes are connected. The time-histories of the area-averaged molecular weight and the specific heat ratio (γ) at the interface between OpenNCC and Glenn-HT are examined (not shown). Although strong unsteady and non-uniform flow fields were observed at the interface, the values of the molecular weight (=28.5) and ratio of specific heats γ (=1.275) remained relatively constant.

These numbers were used in the input of Glenn-HT (used for the entire domain of the interface and the local variations of these values were neglected).

Figures 6 (a)-(c) depict the instantaneous profiles of temperature, axial velocity, and the vorticity when using both OpenNCC (upstream) and Glenn-HT (downstream) where the interface is denoted by the dashed line. In Fig. 6 (a), it is observed that the initialized combustion section is held in a recirculation bubble and then convects downstream where a recirculation zone is over near the interface and flow accelerates in the downstream region. Near the wall, there is a relatively cold region with non-mixed cold air. In addition, it is encouraging to see a smooth propagation of the first derivative (vorticity) from the unstructured mesh

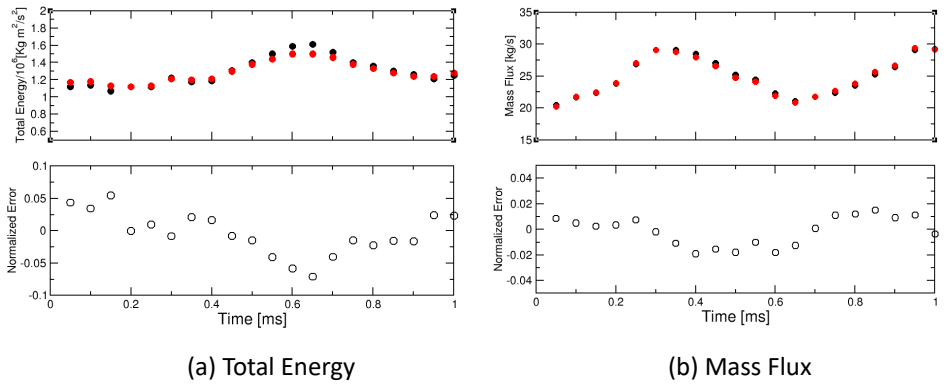

Figure 7. Time-histories of total energy and mass flux at the interface: black: OpenNCC and red: Glenn-GT, and the relative error.

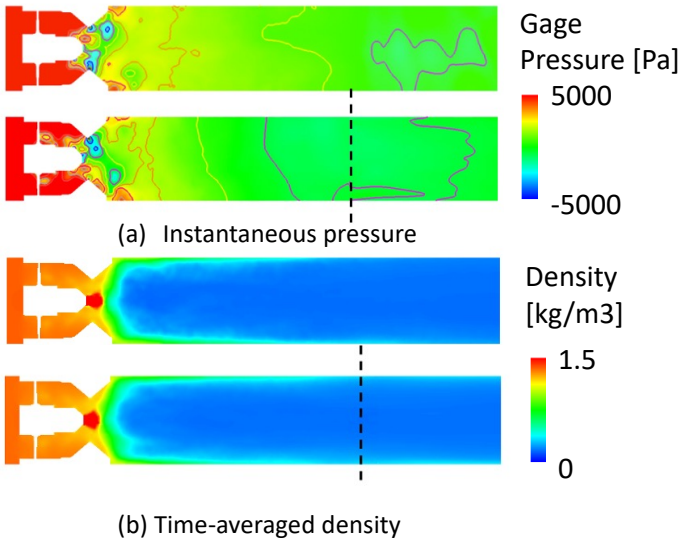

Figure 8. (top) Instantaneous contours of pressure and (bottom) time-averaged contours of density. The dashed line indicates the interface between two domains using OpenNCC and Glenn-HT.

to the structured mesh. Figure 7 shows the time-histories of the mass flux and the total energy recorded before (black: OpenNCC) and after (red: Glenn-HT) the interface. There is up to a 5 and 2 percent error for the mass flux and the total energy, respectively. These errors are due to the hot air with fixed molecular weight and γ imposed in the downstream region. There also appears to be an interpolation error using the interface of the two meshes. Finally, Fig. 8 (a) and Fig. 8 (b) compare the instantaneous pressure profiles and the time-averaged density profiles using (top) OpenNCC only and (bottom) a combination of OpenNCC and Glenn-HT. The interface is denoted by the dashed line. Although there are some discrepancies between the two, overall agreement is satisfactory.

From these results, the conclusion is that the proposed methodology can successfully be used for (non-) reacting applications with reasonable accuracy which use different mesh types with a single interface. In the next subsection, we apply the methodology to simulate the E^3 combustor and HPT in order to investigate the combustor-turbine interactions.

IV. Combustor-Turbine Interactions of E^3 Combustor and HPT

In this section, we investigate the combustor turbine interaction using the geometries of the E^3 combustor and HPT (the General Electric Company version). We consider 24 deg. of the full annular E^3 combustor with the first stage stator of the HPT. Although it is common to impose the pre-described inlet profile for the HPT (e.g.,[52]) (i.e., the profile is obtained by separately simulating the combustor only), the fully-coupled simulation should be able to capture the unsteady flow fields (e.g., combustion dynamics, etc.) more accurately. In a past study, the similar numerical setting was considered .[31] However, the boundary layer was not adequately resolved without the inflation layer in meshing. Thus, the viscus effect as well as the end-wall effect might have been overlooked. Using both the newly generated mesh and Glenn-HT, these effects (and hot streak migration) should be captured more successfully with the updated mesh.

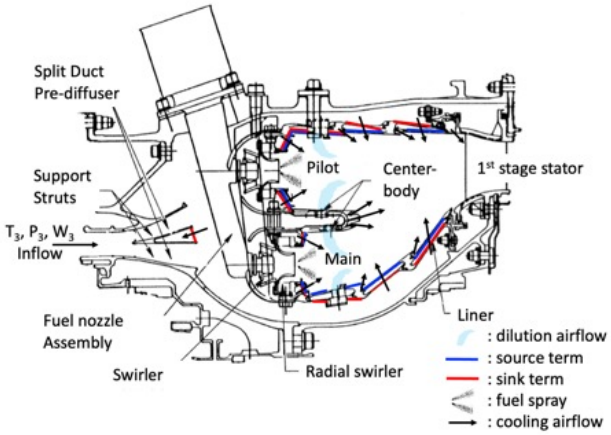

Figure 9. GE-E^3 combustor and high-pressure turbine (first stage stator)[27,29]

A. Geometries of E^3 Combustor and High-Pressure Turbine

The E^3 is the double-annular and compact combustor (see Fig. 9). The main feature of the combustor is an axial primary and radial secondary swirlers, separated by a film-cooled center body. The fuel injected from thirty fuel nozzles combined with the swirling air from the cups are efficiently mixed and combusted in a short distance (0.05 [m]). At a low-power condition, only the outer dome (pilot) is fueled, and a rich combustion zone is formed. At a high-power condition, both domes (main and pilot) are fueled and a large amount of airflow is introduced into the inner dome annulus, creating a very lean combustion zone. The inner and outer lines have two primary dilution holes, designed in such a way that the cold airflow immediately mixes with the hot product, suppressing the further NOx formation. As a simplified experimental setup, the five-cup 60 degree sector combustor design was built and intensively investigated (see Ref.[27]). The E^3 HPT is a two-stage, low through-flow design for moderate loading (only the first stage stator is shown in Fig. 9).

As part of the program,[28,29] the vane configuration was studied based on aerodynamic performance to determine the design point efficiency and to map the turbine over a large range of operating conditions. The aerodynamic design point was the point at the maximum climb. The key aerodynamic parameters of the stage are: tip speed: 514-535 [m/s], numbers of vanes and blades: 46-48, and 76-70, and tip clearance: 0.6-1 [%] of the blade height. In the turbine rig, the simulated hot combustion product was fed at the inlet plane, and thus, the combustor-turbine interactions were out of scope of the test campaign.

B. Numerical Setting: Boundary Condition and Mesh

We considered a realistic Sea-level Takeoff (SLTO) condition and the summary of the condition is shown in Table. 1.

The cooling air flowing through the outer/inner liners and the center body in the combustor are modeled by source/suction terms (i.e, no grids to resolve the cooling holes). The surfaces where we impose the source/sink terms are denoted by blue and red lines in Fig. 9. For other solid walls in the combustor, an adiabatic wall condition is applied. For the wall of the first stage stator, the wall temperature is set to be T_3 (=815 [K]). For modeling the E^3 combustor, we use a reduced chemistry with modified rate coefficients for kerosene– air flames recently developed by Franzelli et al.[53] The reduced chemistry considers five species (i.e., C_aH_b (fuel), O2, CO, H2O, and CO2) and, two following global reactions were proposed:

Table 1. Operating conditions

	$P_{S,41}$ [atm]	$P_{S,45}$ [atm]	T_3 [K]	W_3 [kg/s]	f/a	Wf_{pilot}/Wf_{total}
Test condition	27.4	8.2.	815	3.64	0.0245	0.5

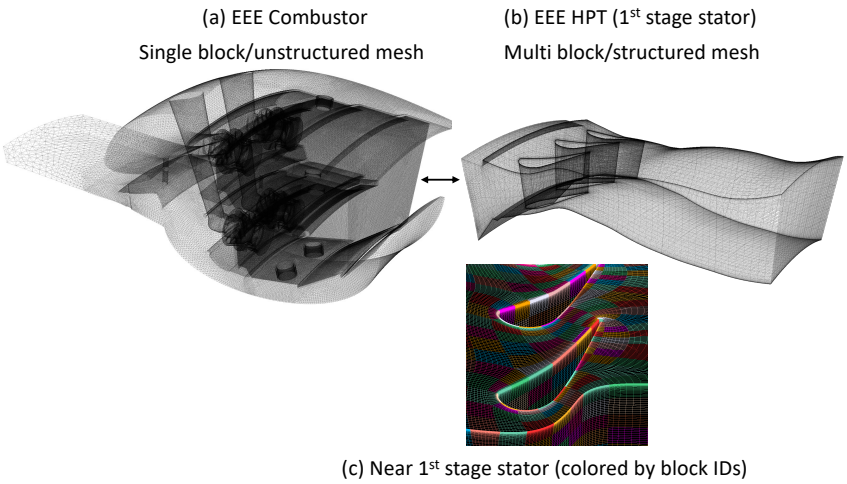

Figure 10. (a) Overview of the combustor, b) the HPT and c) the block ID inside the HPT.

$C_aH_b + (\frac{b}{2}a + \frac{b}{4})O_2 \rightarrow aCO + \frac{b}{2}H_2O$ and $CO + 0.5O_2 \leftrightarrow CO_2$. We consider $C_{11}H_{21}$ as fuel. Liquid fuel is injected as parcels representing a number of real droplets through multiple injection points and in a stochastic manner to mimic a hollow cone distribution. The liquid spray solver is based on a Lagrangian scheme and well-established models for droplet drag and vaporization. A ring of 32 injection points (holes) are located at a radial distance of 3 [mm] from the center point of each fuel nozzle, with 8 individual streams of parcel injected per hole, and a drop size distribution for each stream having a Sauter Mean Diamter (SMD) of 8.8 [μm]. The temperature of a droplet is set to be 515 [K]. Regarding the numerical method, for both OpenNCC and GlennHT, a dual time-stepping procedure in which the solution implicitly advances in physical time and the explicit four-stage Runge–Kutta scheme is called in pseudo time, was adopted. The transport equations are spatially discretized using a cell-centered finite-volume method. The second-order Advection Upstream Splitting Method (AUSM$^+$)-up scheme[42] is used to calculate the inviscid flux minimizing the numerical dissipation.

Figures 10 (a)-(c) show the mesh of the E^3 combustor, the HPT and the closed-up view of the mesh near the 1^{st} stage stator colored by block IDs. For the combustor, the tetrahedral mesh is generated by Cubit, and the total mesh count is about 44 million. The grid sensitivity analysis using the E^3 combustor geometry without the HPT has been done in.[32] It was reported that the fine and uniform grids (average size 0.5mm) inside the combustor, especially within the vicinity of the fuel nozzles and dilution airflows adequately capture the fuel–air mixing and flame structures. For the HPT, the structured mesh is carefully generated with GridPro, and the fine mesh near the solid walls (e.g., stator surface) is used to resolve the boundary layer. The total mesh counts is about 6 million. Please note that Glenn-HT is the multi-block code, and the hundreds of block IDs, each of which has the same element size, are uniquely assigned (See Fig. 10 (c)).

C. Numerical Results

In this subsection, we present numerical results of unsteady calculation using OpenNCC (the E^3 combustor) and Glenn-TH (the E^3 HPT with 1st stage stator) in context of the hot streaks. For this simulation, we use 1080 cores (960 cores for OpenNCC and 120 cores for Glenn-HT) (Xeon E5-2680v2) of Pleiades at the NASA Advanced Supercomputing facilities. First, the time-histories of the area-averaged molecular weight and γ are checked at the combustor exit. It is found that the molecular weight and γ are 29 $\pm$0.05 and 1.275 $\pm$ 0.025, respectively. The molecular weight (=29.0) and γ (=1.275) are used in the input of Glenn-HT.

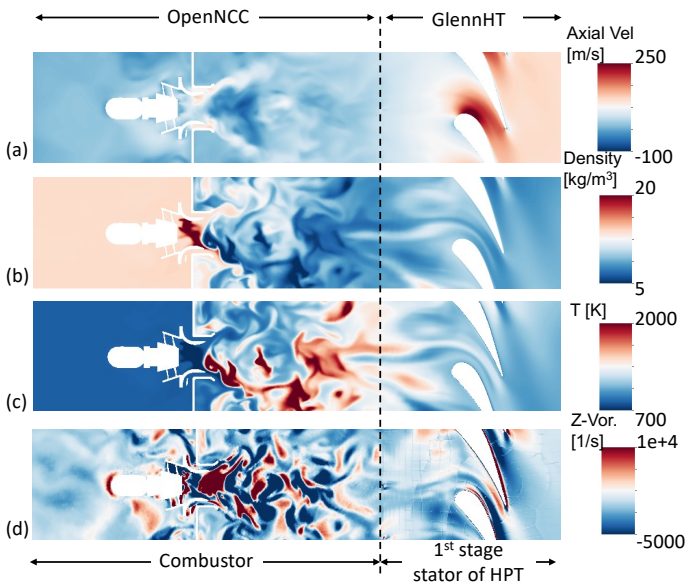

Figure 11. Instantaneous contours of axial velocity, density, temperature and z-component of vorticity. The dashed line indicates the interface between two domains using OpenNCC and Glenn-HT.

Figures 11 (a)-(d) show the snapshots of the instantaneous profiles of axial velocity, density, temperature and the z-component of the vorticity. The dashed line indicates the interface between OpenNCC and Glenn-TH. As expected from this type of combustor, the hot product is held in the central recirculation zone and quickly mixes with the dilution air flows. A variable size of eddies are generated through this mixing process, and the highly non-uniform flow fields are present at the combustor exit. It is observed that all flow properties are smoothly propagated at the interface although the hot-air with the constant molecular weight

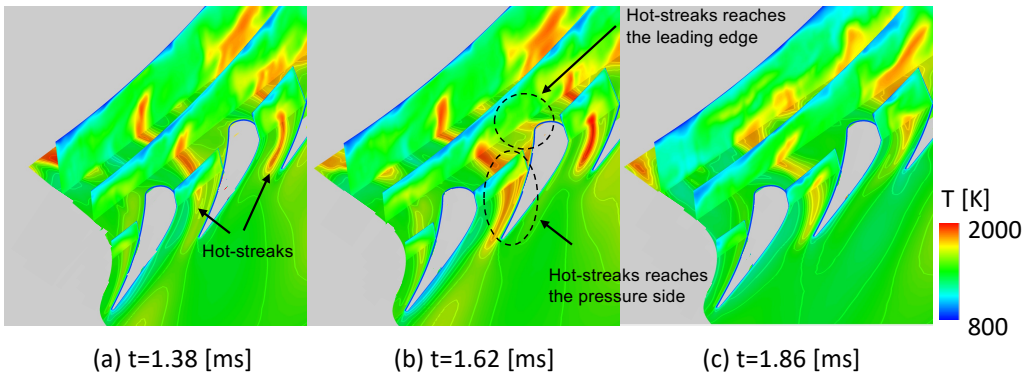

Figure 12. Instantaneous contours of temperature at t=1.38 [ms], 1.62 [ms], and 1.86 [ms]

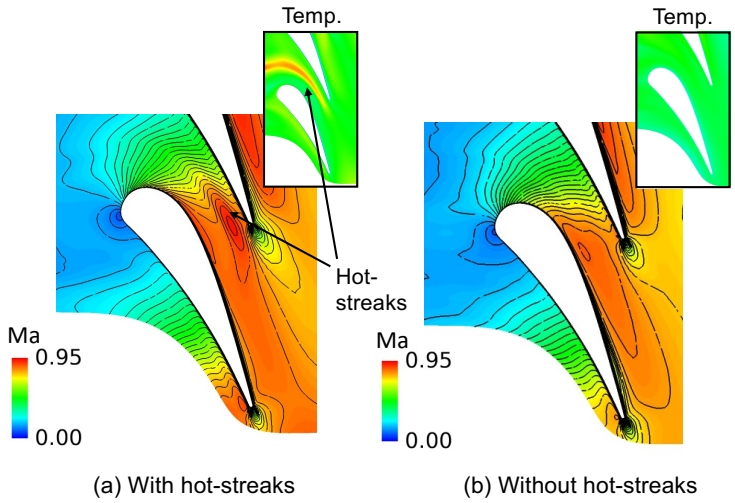

Figure 13. Mach number contours with and without the hot-streak (the inserted figures show the temperature profiles).

and γ is assumed inside the HPT. It is encouraging that the vorticity, which is sensitive to the gradient of the velocity field, smoothly convects between two computational domains. In Fig. 11 (c), it is seen that non-uniform temperature spots (i.e., hot-streaks) are generated in the upstream region of the combustor through the breakup process of a "sheet" of hot products. The sheet is located at the shear layer where the cold spray and hot product mix and combust. The presence of the large dilution airflow seems to be critical in terms of the generation process of such spots. The hot-streaks propagates downstream and reaches the HPT. Figures 12 depict the instantaneous temperature contours at three different time instant (t=1.38 [ms], t=1.62 [ms], and t=1.86 [ms]). At t=1.38 [ms] (see Fig. 12 (a)), there are two hot-streaks passing around the stators. The shapes are elongated due to the flow acceleration. Then, t=1.62 [ms], one of hot-streaks reaches the pressure side of the stator. In addition, a new hot-streak is coming from the upstream and reach the leading edge of the stator. Later (t=1.86 [ms]), although there are still two hot-streaks in the passage, the peak temperature becomes much lower. This specific one course of the hot-steak migration lasts about 0.5 [ms].

Next, we study the effect of hot-streaks on the flowfield inside the passage. While the hot streak travels in the passage between the stators, the temperature of the hot streak quickly drops. It is due to the stretching effect through the flow acceleration as well as the thermal diffusion. In addition, the flow seems to isentropically expand and accelerate while the surrounding pressure decreases. This phenomena has been reported by XXXX Ali, please add your paper!, and our numerical result also clearly captures such an intriguing phenomena. Figure 13 show the instantaneous contour plots of Mach number of two time instants: (a) when the hot-streak is present in the passage and (b) when there is not a hot-streak. When the hot-streak is traveling, there is a locally much higher Mach number region associated with the hot-streak (it looks like a "jet"). The presence of the hot-streak appreciably affects the flowfield as well as the thermal load on the vane.

Another important effect of the hot-streak on the flow field is to affect the vorticity field through a baroclinic torque. The baroclinic torque is a product of the gradients of density and pressure and mathematically defined by : $1/\rho^2 \bigtriangledown\boldsymbol{\rho} \times \bigtriangledown\boldsymbol{p}$. The effect of the baroclinic torque by the hot-streaks could be non-negligible since there are large temperature (i.e., density) and pressure gradients in the passage. Figures 14 (a)-(c) show the snapshots of the instantaneous profiles of the temperature, the magnitude of the baroclinic torque, and the z-component of the vorticity. There is a large non-uniformity in the z-component of the vorticity across the passage, which is caused by the baroclinic torque. It is interesting to see that the strong baroclinic

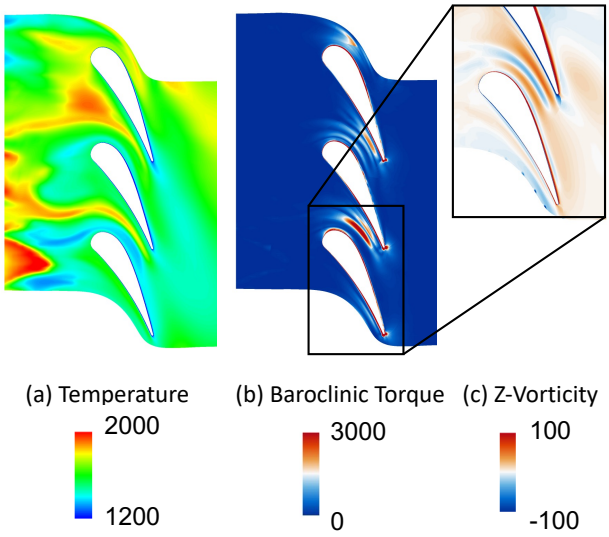

Figure 14. Instantaneous contours of temperature, the magnitude of the baroclinic torque and z-component of vorticity.

torque exists only in the passage region, where the pressure gradient is large. In other words, the effect of the hot-streak on the vorticity field through the baroclinic torque is negligible outside the passage (see the blue regions before and after the stator in Fig. 14 (b)).

Next, as an important part of the combustor-turbine interaction, we investigate the effect of the combustion dynamics on the aerodynamics of the HPT. When the main shows stronger combustion, more cold airflow goes to the pilot and weakens the pilot flame. Once unburnt fuel is accumulated in the pilot, the combustion suddenly takes place in the large volume of the pilot and generates strong pressure waves. This reduces the amount of cold airflow entering to the pilot (i.e., more airflow into the main) and weakens the main. This type of combustion dynamics is problematic particulally for a double-annular combustor like the E^3 design. Figures 15 (a) and (b) show the instantaneous temperature contours at two scenarios when the main/pilot flame dominates. It is observed that when the main shows stronger flame (see Fig. 15 (a)), the bottom half of the combustor is much hotter, and there is a clear difference in the temperature profile at the combustor exit between the top and bottom portions. Figure. 15 (b) shows the similar profile when the pilot flame dominates. With this large non-uniformity in the exit temperature profile, the aerodynamics of the HPT is significantly affected. Figures 16 depicts the instantaneous contour profiles of total pressure (top) and temperature (bottom) at the two cross sections: (top) x=0.36 [m] and (bottom) z=0.0 [m], for two scenarios of the combustion dynamics . After the 1st stage stator (x=0.36 [m]), there is large non-uniformity observed in the total pressure profiles. The dotted circles indicate the wake region of the 1st stage stators, and the distinguished low total pressure spots corresponds to the passage vortices. There are also several local maxima, which are related to the incoming hot-streaks. Compared two results, it is found that the thickness of the boundary layers remarkably differ. When the the main has the stronger combustion, the boundary layer (and cooling airflow) are greatly suppressed. On the other hand, when the pilot flame is stronger, there is a relatively thick cold boundary layer formed at the combustor exit, which leads to the thick boundary layer in the total pressure profile downstream. This kind of unsteady motions of boundary layers as a part of the combustor-turbine interactions could be critical in terms of the aerodynamics of the HPT (e.g., the HPT efficiency) and can be captured only when performing a fully-coupled simulation of the combustor and the HPT.

Figures 17 (a) and (b) show the variations of the normalized velocity magnitude and temperature near the trailing edge. The profiles are recorded along the lines shown in the inserted figures. These files are taken at fifty different time instances, and the averaged values are denoted by the dashed lines. Large

Figure 15. Instantaneous contours of temperature at z = 0.35 [m] when the main/pilot flame dominates.

variations are observed (±12% for the velocity magnitude and ±75% for the temperature). These variations are significantly larger than typical experiments where a simulated hot-streak is introduced at the HPT inlet to investigated the hot-streak migration (e.g., the hot streak temperature ratios are 1.2 for [9] and 1.16 for[16]). Qingjun *et al.*[54] numerically performed a parametric study varying the hot streak temperature ratios from 1.0 to 2.4 while fixing the hot-streak profiles at the HPT inlet. It was observed that with the increase of the hot streak temperature ratio, the relative Mach number and the relative flow angle at the HPT exit increase. Since the current unsteady calculation also predicts high hot streak temperature ratios, such increases in Mach number and flow angle can be expected. More importantly, a fully-coupled simulation should be enable to model the "temporal" variations of these characteristic flow parameters by hot-streaks more accurately. Please note that these variations can be significantly enhanced with the unsteady hot-streak profiles at the inlet, which is overlooked when using the fixed hot-streak profiles.

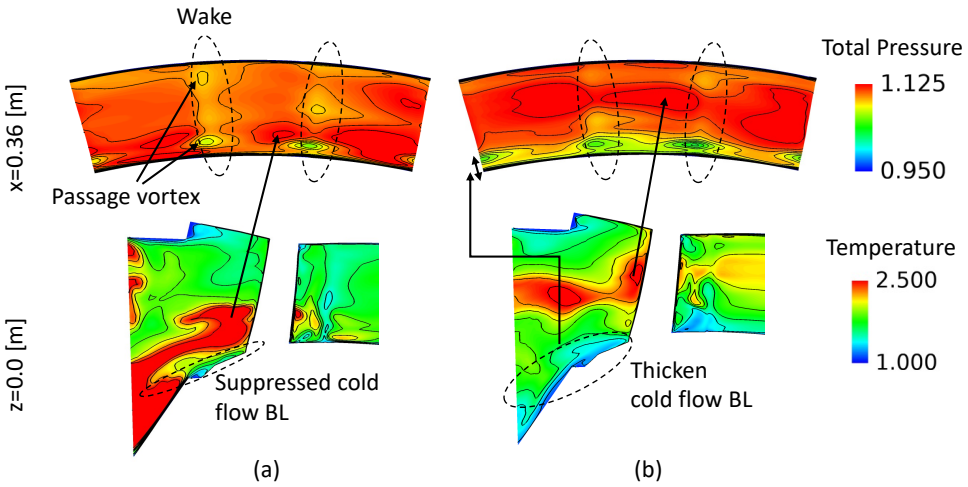

Figure 16. Instantaneous contours of total pressure (top) and temperature (bottom) when the main/pilot flames dominate.

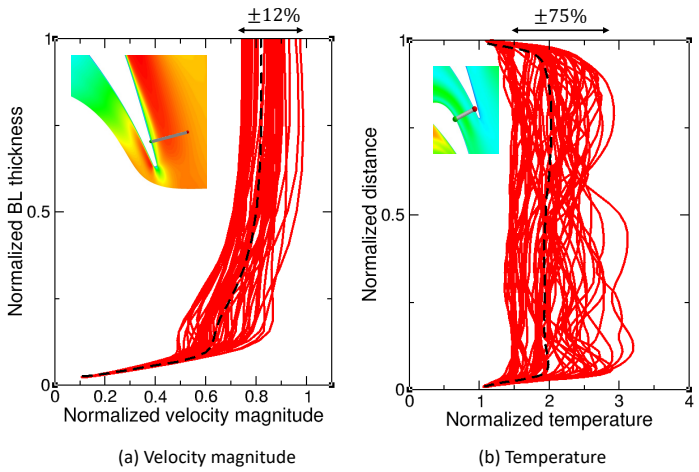

Figure 17. Variation of normalized axial velocity and temperature inside the passage. The dashed lines indicate the averaged profile.

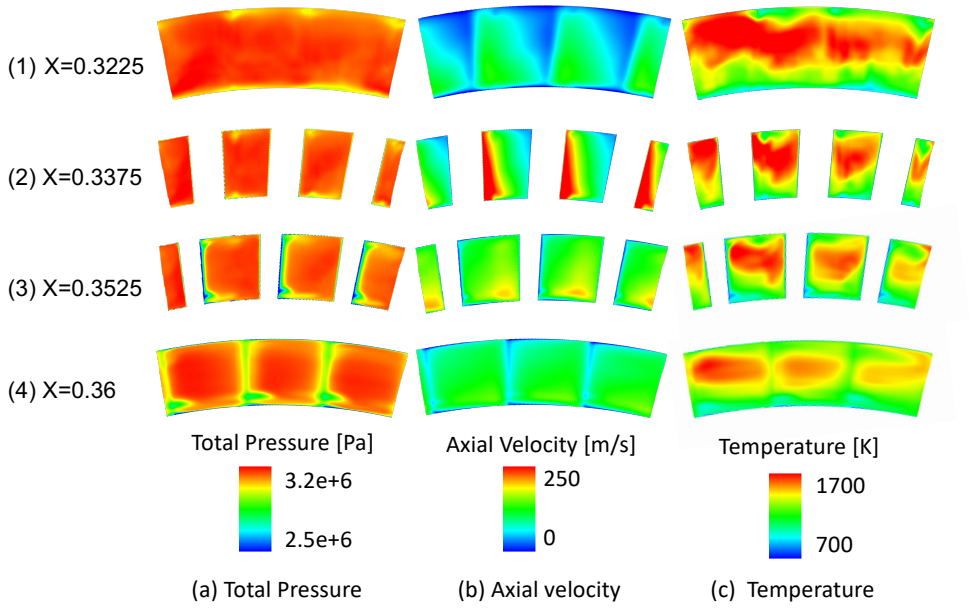

Figure 18. Time-averaged profiles of total pressure, axial velocity and temperature at x = 0.3225 [m], 0.3375 [m], 0.3525 [m] and 0.36 [m].

Finally, we proceed with the analysis of the time-averaged solutions. Figures 18 (a)-(c) show the time averaged total pressure, axial velocity, and temperature at the four different axial locations (x =0.3225 [m], 0.3375 [m], 0.3525 [m], and 0.36 [m]). Highly non-uniform profiles are observed. For instance, relatively high and low total pressure regions exist at x = 0.3225 [m], and these regions are associated with the hot-streaks

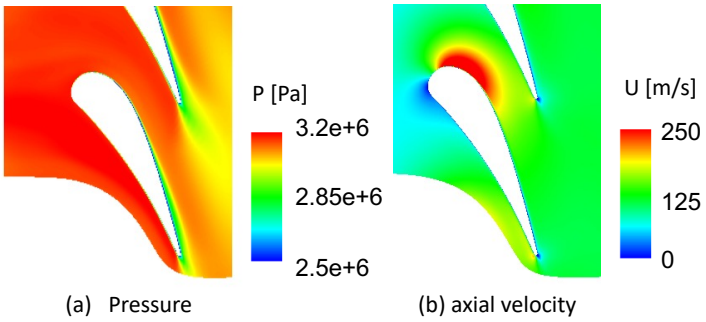

Figure 19. Time-averaged profiles of pressure and axial velocity at y =0.365 [m]

and passage vortices. The area of the low total pressure region near the hub is much larger than the one near the case. This is due to the fact that the pilot flame dominates and the boundary layer near the case is suppressed (this is evidenced by the presence of the hot-streaks near the case). At x = 0.3375 [m], the flow greatly accelerates at the suction side and forms the thick boundary layers downstream (x = 0.3525 [m]). It looks like the boundary layer is separated here. The hot-streaks travel through the passage, and one of hot-streaks remains well even at x = 0.36 [m]. Time-averaged pressure and axial velocity at y = 0.365 [m] are shown in Figs 19 (a) and (b). It is clearly observed that the flow is separated in the middle of the suction side. (However, please note that the flow could be occasionally attached, considering a large variation of the flow fields shown in Fig. 17 (a).)

Based on these observations, we can expect that a fully coupled simulation and a single component simulation would predict the hot-streak migration as well as the aerodynamics inside the HPT in a significantly different way. To optmize the HPT geometries (e.g., shape of blades/vanes, cooling airflow distribution, etc.) for a better efficiency, it might be desirable (or even necessary) to include the combustor as a part of the realistic and accurate inlet condition for the HPT.

V. Conclusions

This paper proposes the coupling methodology of two different CFD codes, OpenNCC and Glenn-HT codes developed at NASA John H. Glenn Research Center, for modeling unsteady flow field and applies the methodology to investigates the combustor-turbine interactions of the E^3 combustor and HPT. First, we performed two test cases for validation and verification of the proposed coupling methodology by modeling the three dimensional backward facing step and the Jet-A/Air combustor with a single learn direct injector. It is confirmed that the coupling methodology works as intended for both test cases. The primary findings from the E^3 combustor and the HPT (1^{st} stage stator) simulation are summarized as follows. Our numerical results indicate the coupling methodology is capable of modeling unsteady non-uniform flow fields at the interface of the combustor exit with satisfactory accuracy although hot air with constant γ and molecular weight is assumed for the HPT. It is found that the combustion dynamics (i.e., the switching main and pilot flame strength) significantly alters the aerodynamic behavior inside the HPT such as the hot-streak migration. It is demonstrated that the Glenn-HT code is capable of capturing the strong air "jet" associated with hot-streaks and that the baroclinic torque plays an important role on the vorticity field in the passage where the noticeable density and pressure gradients exist. Finally, the variations of the velocity magnitude and temperature in the passage are $\pm 12\%$ and $\pm 75\%$, which could be underestimated when the combustor is not included as the HPT inlet condition. Coupling two different CFD codes is challenging especially for unsteady calculations. However, it could be valuable to take an advantage of each code for each computational domain so that overall computational time and accuracy are not compromised compared with a single code calculation.

VI. Acknowledgments

This work was sponsored by the NASA Transformational Tools and Technologies project within the Aeronautics Research Mission Directorate. The authors are also thankful to Dr. Francisco Guzman and Mr. Robert Thacker for editing the paper and Dr. Kumud Ajmani and Dr. Manthenaand Raju for their assistance in preparing and running the simulations. The simulations were conducted on the NASA Advanced Supercomputing (NAS) Pleiades computer cluster. Grid generation was conducted with Cubit (provided by the Sandia National Laboratories) and flow visualization was conducted with Visit (provided by the Lawrence Livermore National Laboratories), respectively.

References

[1]Radomsky, R. and Thole, K. A., "High Free-Stream Turbulence Effects on Endwall Heat Transfer for a Gas Turbine Stator Vane," *Journal of Turbomachinary*, Vol. 122, 2000, pp. 699–708.

[2]Whitney, W. J., Stabe, R. G., and Moffitt, T., "Description of the Warm Core Turbine Facility and the Warm Annular Cascade Facility Recently Installed at NASA Lewis Research Center," Technical memorandum, NASA, 1980, NASA-TM-81562.

[3]Dorney, D. J. and Schwab, J., "Unsteady Numerical Simulations of Radial Temperature Profile Redistribution in a Single-Stage Turbine," *Journal of Turbomachinary*, Vol. 118, 1996, pp. 783–791.

[4]Dorney, D. J., Gundy-Burlet, K., and Sondak, D. L., "A Survey of Hot Streak Experiments and Simulations," *International Journal of Turbo and Jet Engines*, Vol. 816, 1999, pp. 1–15.

[5]Stabe, R. G. and Schwab, J. R., "Performance of a High-Work, Low-Aspect-Ratio Turbine Statot Tested with a Realistic Inlet Radial Temperature Gradient," Technical memorandum, NASA, 1991, NASA-TM-103738.

[6]Butler, T., Sharma, O. P., Joslyn, H. D., and Drings, R. P., "Redistribution of an Inlet Temperature Distortion in an Axial Flow Turbine Stage," *Journal of Propulsion and Power*, Vol. 5, 1989, pp. 64–71.

[7]Basol, A., Jenny, P., Ibrahim, M., Kalfas, A., and Abhari, R., "Hot Streak Migration in a Turbine Stage: Integrated Design to Improve Aerothermal Performance," *Journal of Engineering for Gas Turbines and Power*, Vol. 133, 2011, pp. 061901–1.

[8]Povey, T. and Qureshi, I., "A Hot Hot-Streak (Combustor) Simulator Suited to Aerodynamic Performance Measurements," *Proceedings of the Institution of Mechanical Engineers, Part G: Journal of Aerospace*, Vol. 222, 2008, pp. 705–720.

[9]Quresh, I., Bereta, A., and Povey, T., "Effect of Simulated Combustor Temperature Nonuniformity on HP Vane and Enf Wall Heat Transfer: An Experimentral and Computational Invesitgation," *Journal of Turbomachinery*, Vol. 133, 2011, pp. 031901.

[10]Hall, B., Chana, F., and Povey, T., "Design of a Nonreacting Combustor Simulator With Swirl and Temperature Distortion With Experimental Validation," *Journal of Engineering for Gas Turbines and Power*, Vol. 136, 2014, pp. 081501–1.

[11]Adams, M., Beard, P., Stokes, M., Wallin, F., Chana, K., and Povey, T., "Effect of a Combined Hot-Streak and Swirl Profile on Cooled 1.5- Stage Turbine Aerodynamics: An Experimental and Computational Study," *Journal of Turbomachinary*, Vol. 143, 2021, pp. 02101.

[12]Jacobi, S., Mazzoni, C., Rosic, B., and Chana, K., "Investigation of Unsteady Flow Phenomena in First Vane Caused by Combustor Flow With Swirl," *Journal of Turbomachinary*, Vol. 139, 2017, pp. 041006.

[13]Barringer, M., Thole, K., Polanka, M., Clark, J., and Koch, P., "Migration of Combustor Exit Profiles Through High Pressure Turbine Vanes," *Journal of Turbomachinary*, Vol. 131, 2009, pp. 021010–1.

[14]Camille, B., Friedrich, K., Nick, A., William, P., Michael, O., Caciolli, G., Tarchi, L., Mersinligil, M., and Raffel, J., "Full aerothermal combustor turbine interaction research," 2012.

[15]Bacci, T., Facchini, B., Picchi, A., Tarchi, L., Koupper, C., and Champion, J.-L., "Turbulence Field Measurements at the Exit of a Combustor Simulator Dedicated to Hot Streaks Generation," *Proceedings of the ASME Turbo Expo*, Montreal, Canada, June 2015, GT2015-42218.

[16]Koupper, C., Gicquel, L., Duchaine, F., Bacci, T., Facchini, B., Picchi, A., Tarchi, L., and Bonneau, G., "Experimental and Numerical Calculation of Turbulent Timescales at the Exit of an Engine Representative Combustor Simulator," *Journal of Engineering for Gas Turbines and Power*, Vol. 138, 2016, pp. 021503–1.

[17]Andreini, A., Facchini, B., Insinna, M., Mazzei, L., and Salvadori, S., "Hybrid RANS-LES Modeling of a Hot Streak Generator Oriented to the Study of Combustor-Turbine Interaction," *Proceedings of the ASME Turbo Expo*, Montreal, Canada, June 2015, GT2015-42402.

[18]Andreini, A., Bacci, T., Insinna, M., Mazzei, L., and Salvadori, S., "Hybrid RANS-LES Modeling of the Aerothermal Field in an Annular Hot Streak Generator for the Study of Combustor–Turbine Interaction," *Journal of Engineering for Gas Turbines and Power*, Vol. 139, 2017, pp. 021508.

[19]Duchaine, F., Dombard, L, J., Gicquel, L. M., and Koupper, C., "On the importance of inlet boundary conditions for aerothermal predictions of turbine stages with large eddy simulation," *Computers & Fluids*, Vol. 154, 2017, pp. 60–73.

[20]Schluter, J., Apte, S., Kalitzin, G., Weide, V., Alonso, J. J., and Pitsch, H., "Large-scale integrated LES-RANS simulations of a gas turbine engine," *Proceedings of Center for Turbulence Research Annual Research Briefs*, Stanford, CA, 2005.

[21]Medic, G., Kalitzin, G., You, D., Weide, E., and J. Alonso, a. H. P., "Integrated RANS/LES Computations of an Entire Gas Turbine Jet Engine," *Proceedings of the 45th AIAA Aerospace Sciences Meeting and Exhibit*, January 2007, AIAA Paper 2007-1117.

[22]Verma, I., Basani, J., Zori, L., and Rida, S., "Modeling of Combustor and Turbine Vane Interaction," *Proceedings of the ASME Turbo Expo*, Phoenix, AZ, USA, June 2019, GT2019-90325.

[23]Roux, S., Cazalens, M., and Poinsot, T., "Outlet-Boundary-Condition Influence for Large Eddy Simulation of Combustion Instabilities in Gas Turbines," *Journal of Propulsion and Power*, Vol. 24, 2008, pp. 541–546.

[24]Xia, G., Kalitzin, G., Lee, J., Medic, G., and Sharma, O., "Hybrid RANS/LES Simulation of Combustor/Turbine Interactions," *Proceedings of the ASME Turbo Expo*, Virtual, September 2020, GT2020-14873.

[25]Gründler, J., S. H.-P. and Lehmann, K., "An Efficient Unsteady 1-Way Coupling Method of Combustor and Turbine," *Proceedings of the ASME Turbo Expo*, Rotterdam, The Netherlands, June 2022, GT2022-78056.

[26]Miki, K., W. T. and Moder, J., "Computational Study on Fully Coupled Combustor–Turbine Interactions," *Journal of Propulsion and Power*, 2023, doi.org/10.2514/1.B38501.

[27]Burrus, D.-L., C'hahrour, C. A., Foltz, H. L., Sabia, P. E., Seto, S. P., and Taylor, J. R., "Energy Efficient Engine Combustor Test Hardware Detailed Design Report," Technical Reports Server (NTRS), NASA, 1984, NASA-CR-20643.

[28]Halila, E. E., Lenahan, D. T., and Thomas, T., "Engine High Pressure Turbine Test Hardware Detailed Design," Technical Reports Server (ntrs), NASA, 1982, NASA-CR-16795.

[29]Timko, L. R., "Energy Efficient Engine High pressure Turbine Component Test Pefformance Report," Technical Reports Server (NTRS), NASA, 1984, NASA-CR-168289.

[30]Miki, K., Moder, J., and Liou, M.-S., "Enhancing Open National Combustion Code and Application of Energy Efficient Engine Combustor," *Journal of Propulsion and Power*, Vol. 34, 2018, pp. 415–427.

[31]Miki, K., Moder, J., and Liou, M.-S., "Computational study of combustor–turbine interactions," *Journal of Propulsion and Power*, Vol. 34, 2018, pp. 1529–1534.

[32]Miki, K., Moder, J., and Liou, M. S., "AUSM scheme: its application to a realistic combustor configuration, the Energy Efficient Engine," *Shock Waves*, Vol. 29, 2019, pp. 1009–1021.

[33]Zhang, Y. and Lei, K., "3D Multi-Solver Coupled Simulation of Combustor-Turbine Interaction in an Aero-Engine," *Proceedings of the ASME Turbo Expo*, Virtual, June 2020, GT2020-14540.

[34]Kim, W.-W. and Menon, S., "A new dynamic one-equation subgrid-scale model for large eddy simulations," *Proceedings of the 33rd AIAA Aerospace Sciences Meeting and Exhibit*, January 1995, AIAA Paper 1995-356.

[35]Pope, S. B., "PDF Methods for Turbulent Reactive Flows," *Progress in Energy and Combustion Science*, Vol. 11, 1985, pp. 119–192.

[36]Fuereby, C. and Lofstrom, C., "Large-Eddy-Simulation of Bluff-Body Stabilized Flames," *Symposium (International) on Combustion*, Vol. 25, 1994, pp. 1257–1264.

[37]Legier, J. P., Poinsot, T., and Veynante, D., "Dynamically Thickened Flame LES model for Premixed and Non-Premixed Turbulent Combustion," *Proceedings of Proceedings of the Summer Program*, 2000, Center for Turbulence Research, Stanford University.

[38]Gallagher, T., *A Generalized Maccormack Scheme for Low Mach Number, Chemically-Reacting Large-eddy Simulations*, PhD Thesis, Georgia Institute of Technology, Atlanta, GA, June 2017.

[39]Menon, S. and Kerstein, A., "Stochastic Simulation of the Structure and Propagation Rate of Turbulent Premixed Flames," *Symposium (International) on Combustion*, Vol. 24, 1992, pp. 443–450.

[40]Raju, M., "LSPRAY-II: A Lagrangian Spray Module," Technical Reports Server (NTRS), NASA, 2013, See ISBN-13: 978-1289158569.

[41]Steinthorsson, E., Liou, M.-S., and Povinelli, L., "Development of an Explicit Multiblock/Multigrid Flow Solver for Viscous Flows in Complex Geometries," *Proceedings of the 29th Joint Propulsion Conference and Exhibit*, June 1993, AIAA Paper 1993-2380.

[42]Liou, M.-S., "A Sequel to AUSM: AUSM$^+$," *Journal of Computational Physics*, Vol. 129, 1996, pp. 364–382.

[43]Shih, T.-H. and Liu, N.-S., "Modeling of Internal Reacting Flows and External Static Stall Flows Using RANS and PRNS," *Flow, Turbulence and Combustion*, Vol. 81, 2008, pp. 279–299.

[44]Menter, F., "Zonal Two-Equation $k-\omega$ Turbulence Models for Aerodynamic Flows," *Proceedings of the AIAA 23rd Fluid Dynamics, Plasmadynamics, and Lasers Conference*, Orlando,FL, 1993, AIAA1993-2906.

[45]Wilcox, D., "Simulation of Transition With a Two-Equation Turbulence Model," *AIAA Journal*, Vol. 32, 1994, pp. 255–274.

[46]Wei, L., Ge, X., George, J., and Durbin, P., "Modeling of Laminar-Turbulent Transition in Boundary Layers and Rough Turbine Blades," *Journal of Turbomachinery*, Vol. 139, 2017, pp. 111009–1.

[47]Ameri, A., Shyam, V., Rigby, D., Poinsatte, P., and Thurman, D., "Development of the Glenn-Heat-Transfer (Glenn-HT) Computer Code to Enable Time-Filtered Navier Stokes (TFNS) Simulations and Application to Film Cooling on a Flat Plate Through Long Cooling Tubes," *Proceedings of AIAA Propulsion and Energy Forum*, Cleveland, OH,, July 2014, AIAA2014-07-28.

[48]Ameri, A., "Implicit-LES Simulation of Variable-Speed Power Turbine Cascade for Low Free-Stream Turbulence Conditions," *Proceedings of the ASME Turbo Expo*, Oslo, Norway,, June 2018, GT2018-77120.

[49]Miki, K. and Ameri, A., "Large-Eddy Simulation of Variable Speed Power Turbine Cascade With Inflow Turbulence," *Journal of Turbomachinery*, Vol. 143, 2020, pp. 081006.

[50]Ameri, A., Rigby, D., Steinthorsson, E., Heidmann, J., and Fabian, J., "Unsteady Analysis of Blade and Tip Heat Transfer as Influenced by the Upstream Momentum and Thermal Wakes," *Journal of Turbomachinery*, Vol. 132, 2010, pp. 041007.

[51]Driver, D. M. and Seegmiller, H. L., "Features of Reattaching Turbulent Shear Layer in Divergent Channel Flow," *AIAA Journal*, Vol. 23, 1985, pp. 163–171.

[52]Miki, K., Wey, T., and Moder, J., "Numerical Study of Combustor-Turbine Interactions considering a Two-Stage High-Pressure Turbine," *Proceedings of the International Society for Air Breathing Engines*, Canberra, Australia, Sept. 2019, ISABE-2019-24396.

[53]Franzelli, B., Riber, E., Sanjose, M., and Poinsot, T., "A Two-step Chemical Scheme for Kerosene-Air Premixed Flames," *Combustion and Flame*, Vol. 3, 2010, pp. 1364–1373.

[54]Qingjun, Z., Huishe, W., Xiaolu, Z., and Jianzhong, X., "Numerical Investigation on the Influence of Hot Streak Temperature Ratio in a High-Pressure Stage of Vaneless Counter-Rotating Turbine," *International Journal of Rotating Machinery*, Vol. 2007, 2007, pp. 056097.